



Ultrasensitive paper-based polyaniline/graphene composite strain sensor for sign language expression

Qiuping Qian^{a,b,1}, Yan Wang^{c,1}, Min Zhang^a, Limin Chen^{a,b}, Jie Feng^{a,b}, Yi Wang^{a,b,**}, Yunlong Zhou^{a,b,*}

^a School of Ophthalmology and Optometry, Eye Hospital, School of Biomedical Engineering, Wenzhou Medical University, Wenzhou, 325000, PR China

^b Engineering Research Center of Clinical Functional Materials and Diagnosis & Treatment Devices of Zhejiang Province, Wenzhou Institute, University of Chinese Academy of Sciences, Wenzhou, 325000, PR China

^c Department of Materials Science & Engineering, Southern University of Science & Technology, Shenzhen, Guangdong, 518055, PR China

ARTICLE INFO

Keywords:

Paper-transferring
Ultra-sensitivity
Micro-disconnection
Micro-cracking

ABSTRACT

We report a facile, low cost and readily scalable method for the fabrication of a flexible paper-based strain sensor. Approaches of pen-writing, paper-transferring and elastomer-packaging were exploited to build a strain sensor with layered structures consisting of the graphene mesh and conductive polyaniline. The normalized conductivity change ($\Delta G/G_0$) and gauge factor could reach as high as 747 and 1.1×10^4 , respectively. The mechanism of ultra-high conductivity change was attributed to the formation of micro-disconnection and micro-cracking in the layered structure deduced by Raman imaging and a simulation based on equivalent resistor networks. As a proof of the concept, the strain devices were finally exploited in sign language recognition. Our work demonstrated a new strategy to create ultra-high sensitive communication devices for people with speech and hearing impairment.

1. Introduction

The rapid development of nanotechnology provides a platform for constructing innovative health monitoring devices [1,2]. For example, by integrating traditional lithography and micro-fabrication, nanomaterials can be assembled into multifunctional flexible devices, which can detect body signals through monitoring pulse, heartbeat, breath, blink and so on [3–5]. To date, a variety of flexible devices have been reported with various detection schemes, such as mechanical, thermal, chemical, photic, electrical principles [6–9]. Strain-based flexible devices, particularly, have found wide applications in health monitoring, which detect the electric changes upon mechanical deformations such as stretching, compression, shear, etc [10–12]. Recently, various flexible strain sensors have been fabricated by employing nanomaterials including metallic nanomaterials, semiconductors, carbon nanotubes, graphene, and conductive polymers [13–21]. Strain sensors capable of detection of high or low strain are in demands for unprecedented applications. For example, a wearable strain sensor can be used to develop

healthcare products by monitoring joint movements when wearing on knees, hands, elbows and finger joints [22–29].

Three crucial factors were commonly used to evaluate the strain sensor, i.e. process-operability, flexibility, and sensitivity. However, it remains a significant challenge to fabricate flexible strain sensors with high sensitivity through simple processing. High flexibility requires materials to maintain their structural and morphological integrity under applied strain. Generally, a high sensitivity of strain sensor means large structural change under the strain [30,31]. Sensitivity is often measured by gauge factor (GF), which is expressed in Equation (1)

$$GF = \frac{\Delta R/R_0}{\epsilon} \quad (1)$$

where the $\Delta R/R_0$ indicates the relative change in resistance and ϵ indicates the mechanical strain, respectively. Strain sensor based on metal nanowires can achieve good stretchability, however, its GF is typically in a low range of 3–40 [32]. Conductive polymer-based sensor shows both good flexibility and sensitivity. Technically, conductive polymer

* Corresponding author. School of Ophthalmology and Optometry, Eye Hospital, School of Biomedical Engineering, Wenzhou Medical University, Wenzhou, 325000, PR China.

** Corresponding author. School of Ophthalmology and Optometry, Eye Hospital, School of Biomedical Engineering, Wenzhou Medical University, Wenzhou, 325000, PR China.

E-mail addresses: wangyi@wibe.ac.cn (Y. Wang), zhouyl@wibe.ac.cn (Y. Zhou).

¹ These two authors contribute equally to this work.

as a softer electrode/sensing material also possess many advantages including easily processed and modified properties [33–35]. For example, polyaniline (PANI), the conductivity of which could be adjusted by doping with acid, provided a strategy for increasing the signal-to-noise ratio and sensitivity [36,37]. PANI-based strain sensor could withstand strain up to 50% with a GF up to 54 [38]. Strain sensor composed of stacked conductive polymer and carbon nanotubes nanohybrid film could achieve sensitivity with GF up to 62.3 [39]. However, the fabrication of the composite films for this sensor is technically complex. Alternatively, strain sensor based on doping conductive polymer microparticles into gold nanowire films can form the sea-island structure, leading to several-fold improvement in sensitivity comparing to typical strain sensors. The soft and elastic gold nanowires matrix can absorb reversibly external forces to form micro-crack under strain, which is responsible for the decrease of conductive pathways, hence increasing the overall electrical resistance, the GF could reach 61.4 at large strain of 100% [40]. Recent study suggested that strain sensor based on two dimensional nanomaterials showed high sensitivity, which mainly originated from the morphology change of strain-dependent layered percolative film. Upon straining, neighboring flakes of two dimensional nanomaterial reversibly lose their contact, and form breakage of percolation pathways at microscale, as a result, the GF can reach up to 150 [41]. In addition, it is well known that state of the art of reduce graphene oxide based flexible sensors typically include patterning by highly cost photolithography and time-consuming layer-by-layer assembly method [42], transferring of pattern chemical vapor depositions-grown graphene films with a few of layers to the hierarchical structured PDMS film is also technically challenge [43].

In this contribution, we designed a strain sensor with a sandwich structure composed of graphene meshes (GM) and polyaniline (PANI) deposited on a flexible paper. This GM/PANI composite endows good stability, large flexibility and ultra-sensitivity to the strain sensor. Our strategy presents several key advantages: Firstly, it is easy to manipulate the fabrication of strain sensor based on the pen-writing, paper-transferring and elastomer-packaging. Secondly, the sensitivity of the sensor can be facily regulated and controlled by the composition of PANI and GM. Due to the special junction structure and the formation of micro-disconnection and micro-cracking of the composite material, the sensor has an ultra-high sensitivity, in which GF can reach up to 1.1×10^4 . Thirdly, the sensor maintains good stability, flexibility and ultra-sensitivity even after 1000 cycles of testing.

2. Experimental details

2.1. Materials

Filter paper (diameter ~ 15 cm) was purchased from Whatman Company. A writing brush (Beijing jinghua brush factory) was used for pen-writing fabrications. $\text{FeCl}_3 \cdot 6\text{H}_2\text{O}$ (99% purity), Aniline (99% purity) were purchased from Shanghai Aladdin Co., Ltd. Concentrated HCl solution (36–38 wt %) was purchased from Beijing Chemical Reagent Company. Deionized water ($18.2 \text{ M}\Omega \text{ cm}^{-1}$) was obtained from a Milli-Q water-purification System. Sylgard 184 (Polydimethylsiloxane) was purchased from Dow Corning Company. Silver wire (99.97% purity and diameter ~ 0.3 mm) was obtained from Denmark Jensen Company. Conductive Silver Paint was purchased from SPI-CHEM Company.

2.2. Characterization and electrical measurements

A commercial digital camera was applied to acquire some distinct and macroscopic pictures. SEM images were captured on a Hitachi Su 8010 instrument at a voltage of 3.0 kV. Microscope images were captured on a Nikon Ni-U Upright Microscopy. The Raman spectra was recorded with a Raman system with a double-frequency Nd:YAG laser (512 nm) as the excitation source. Raman images were captured on a

Renishaw Invia Raman microscope. The electrical conductivities of the strain sensors were generally measured by a digital source meter (Keithley 2602), and the Source-Drain voltage with 1 V DC bias. The tensile test was carried out on a compressing and stretching machine (Instron 5943).

2.3. Fabrication of filter paper deposited by PANI

A piece of circular filter paper was manually written with FeCl_3 (3 M, pH 1) by the writing brush and subsequently covered onto a culture dish containing a certain amount of aniline. The conductive papers were taken off after polymerization at room temperature. Then the conductive papers were washed several times by alcohol and water.

2.4. Synthesis of GM

Copper meshes (100 mesh, wires of 100 μm in diameter) were cleaned, tailored, and pretreated as presented. As the temperature reached 1000 $^\circ\text{C}$, H_2 was turned down to $8 \text{ cm}^3 \cdot \text{min}^{-1}$, CH_4 ($38 \text{ cm}^3 \cdot \text{min}^{-1}$) was introduced into the reactor at ambient pressure. And Ar was cut off for 1 min, and then turned up to $200 \text{ cm}^3 \cdot \text{min}^{-1}$. After 35 min growth, the mesh was rapidly cooled down to room temperature. Graphene was grown around the copper mesh. Finally GM could be obtained by removing the copper mess, which was etched away by an aqueous solution of FeCl_3 (0.5 mol L^{-1}) and HCl (0.5 mol L^{-1}).

2.5. Fabrication of flexible strain sensor with a fresh sandwich structure

The PDMS mixture of base and cross-linker (the weight ratio of base to crosslinker was 10:1) was stirred at least for 15 min. The medical tape was attached evenly on a clean disposable plastic Petri dish, and then PDMS mixture was spin-coated onto the medical tape gently, degassed in vacuum for 30 min to remove bubbles at room temperature, solidified at 80 $^\circ\text{C}$ for 2 h, and peeled off from the Petri dish to get the composite PDMS-medical tape film (≈ 0.5 mm thick). After transferring and drying the GM on paper-based PANI-PDMS-medical tape film, silver wires were connected using silver paste to form the GM-PANI-PDMS-medical tape strain sensor. PDMS glue was used for covering the electrodes to protect them from exfoliating, and then the multiple devices were assembled.

2.6. Flexibility and sensing tests

The flexibility test was followed on a digital source meter at a given voltage of 1.0 V. The response of the sensor was followed by the normalized change of conductivity, $\Delta G/G_0$, which was calculated by the normalized change of current,

$$\Delta G/G_0 = -(I - I_0)/I_0 = [(R - R_0)/R_0]$$

where G_0 , I_0 , and R_0 , are the initial conductivity, current and resistance before the sensing test, and I and R is the current and resistance under the strain.

2.7. Fracture model and resistance prediction of GM/PANI sensor upon the strains

To investigate the effect of the fracture of GM/PANI sensors, a program was developed to achieve the relationship between the resistance of GM/PANI and the strain. The program employs the technique of nodal analysis to form the linear equation system [16]. With other sparse matrix functions of MATLAB, this program is able to efficiently handle strain sensor and provide a convenient tool to estimate the GM/PANI's resistance for the specified micro-cracking density. Because the GM with crisscross meshes structure is evenly flatted out on the PANI filter paper, we assume there are many series and parallel circuits of the sensor. Therefore, GM and PANI can be chopped up into

many equivalent resistance elements as building blocks. It can be modeled as the 2D resistor network as shown in Fig. S9. In this model, due to the formation of micro-disconnections and micro-crackings, the resistance value of GM's and PANi's resistance elements evenly changed under different strains. Under the low strain (2–4%), the formation of micro-disconnections enables some GM's and PANi's resistance elements evenly increase a little. Thus the distributed resistance of the sensor moderately increase to higher equivalent resistance. Under the higher strain (5–7%), more micro-disconnections and micro-crackings are formed, thus, more GM and PANi's resistance elements of intersections/connections continually increased. Therefore, the corresponding calculated normalized conductivity changes (NCCs) can be achieved by a quasi-equivalent resistor network model.

3. Results and discussion

3.1. Fabrication of flexible PANi/GM paper-based strain sensor

First and foremost, a low cost and simple preparation method to build flexible strain sensors is highly demanded. Pen-writing is easy to operate and without specific requirement for the ink, which provides great possibility for practical use [43,44]. Here, pen-writing PANi/GM on filter paper was fabricated as illustrated in Fig. 1. The writing started with a brush filled with 3 M FeCl_3 solution, which was later scribbled on the filter paper with a diameter of 90 mm. Then, the filter paper with FeCl_3 was exposed to aniline vapor, giving rise to rapid interfacial polymerization of PANi. Fig. 1b showed the paper-transferring and elastomer-packaging process for the fabrication of the strain sensor. GM was grown by atmospheric pressure chemical vapor deposition (CVD) on the surface of crisscross copper meshes. Subsequently, the copper meshes were etched away in FeCl_3/HCl solution, and then GM was transferred to the filter paper deposited with PANi. After that, GM/PANi papers were attached to a PDMS film covered with medical tape.

The GM/PANi layers were connected to silver wires with silver paste on both ends and finally covered with a thin layer of PDMS for the protection of electrodes.

Two major factors were considered to optimize the design, one is the polymerization of PANi and the other is the line width of GM. The effect of polymerization time on PANi's conductivity was first evaluated. While increasing the polymerization time from 0.5 to 2 h, the resistance of PANi filter paper continuously declined down to $9.7 \text{ k}\Omega \text{ sq}^{-1}$. With the further extension of the polymerization time from 2 to 3 h, the resistance basically remained unchanged. Therefore, a polymerization time below 2 h was selected to fabricate the conductive PANi filter paper. A deep blue color appeared on the filter paper upon the deposition of PANi (Fig. S1). Then the width of GM/PANi/paper sensor was further selectively considered to optimize the strain sensitivity, and all the sensors have the same length of 20 mm.

3.2. Performance of GM/PANi/paper sensor

To quantify the sensing ability under specific strain, the signal output was normalized by the conductivity change $\Delta G/G_0$ as expressed in Equation (2):

$$\Delta G/G_0 = (R - R_0)/R_0 \quad (2)$$

where ΔG is the initial conductivity and R_0 is resistance before the applying of strain, respectively, and R is the resistance under the applied strain. We found that narrowing the width of the sensor chip can dramatically improve the strain sensitivity. The normalized conductivity change for a 5 mm width shows six times higher than that of 15 mm width under 5% strain. However, its electrical response indicates limited stability upon 6 cycles of measurements (Fig. S2). The sensitivity of the sample with 15 mm width is only 50% of the 10 mm ones. Therefore, we chose the sensor array with a width of 10 mm for the following design.

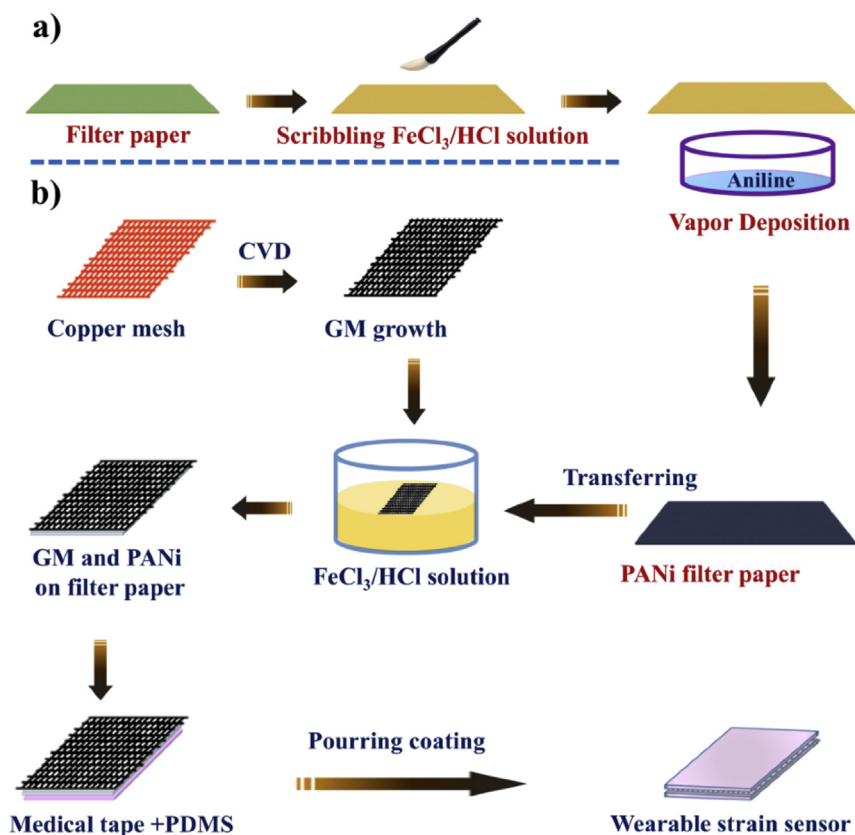


Fig. 1. Schematic illustration of the fabrication of flexible PANi/GM paper-based strain sensor.

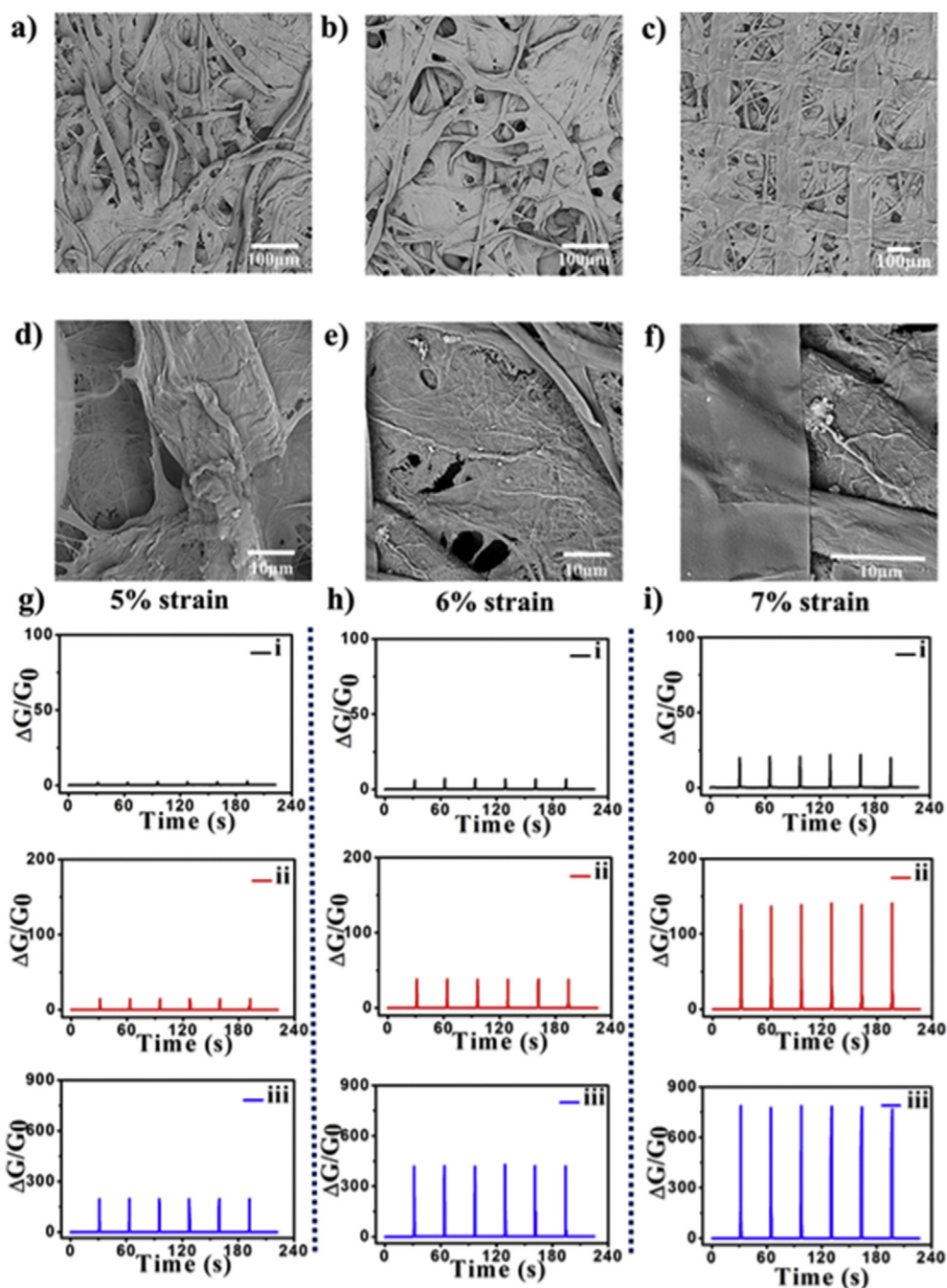


Fig. 2. SEM images of filter paper (a, d), filter paper coated with PANi upon 2 h polymerization (b, e), and filter paper coated with PANi and GM (c, f). The NCC of PANi/paper sensor (i), GM/paper sensor (ii) and GM/PANi/paper sensor (iii) (g: 5% strain, h: 6% strain, i: 7% strain).

Pen-writing PANi provides the feasibility of filter paper to serve as a flexible device substrate with conductive circuits. The SEM images in Fig. 2 indicated that the PANi was embedded in the filter paper with fiber-crossing structure. While the GM with crisscross meshes structure can be seen on the PANi-coated filter paper, the mechanical property of GM/PANi/paper was robust enough for large-scale preparation, as illustrated in Fig. 2c-f. For example, a slice of 80 mm × 80 mm GM-PANi-filter paper can produce almost 32 slices of GM/PANi/paper sensors with 20 mm length, 10 mm width (Fig. S3a). Due to the strong van der Waals force between elastomeric matrix (PDMS) and conductive fillers (GM/PANi), the GM/PANi/paper sensors possess satisfactory flexibility and stability. As shown in Fig. S3b, the strain sensor has good adhesion property on human hands, demonstrating the wearable and flexible features.

In order to evaluate the performance of GM/PANi/paper sensor, we compared its sensitivity with PANi/paper and GM/paper sensors. Five different strains, i.e. 2%, 4%, 5%, 6% and 7% (Table S1), were applied to investigate their impact on the NCC of sensors at a testing frequency of 1 Hz. The NCC value of PANi/paper sensor is basically zero under 2% and 4% strain. The NCC for GM/PANi/paper and GM/paper strain sensors is almost the same value, i.e. 2 under 2% strain. The GM/PANi/paper sensor's NCC is 16 under 4% strain, which is two times higher than that of the GM/paper sensor (Fig. S4). Under the strain from 5% to 7%, the NCC for PANi/paper sensor increased from 3 to 22 and the NCC for GM/paper sensor increased from 15 to 138 (Fig. S5), respectively. More surprisingly, the NCC value for GM/PANi/paper sensor's is 198, 420 and up to 800 under 5%, 6% and 7% strain. Noteworthy, the NCC value of the GM/PANi/paper sensor is ~800 under 7% strain, which is

about six times and thirty-six times higher than the GM/paper and PANi/paper sensors, as shown in Fig. 2i.

3.3. Mechanism of building high strain gauges

Strain-resistance response of sensor gauges mainly arise from two aspects: one is intrinsic piezo-resistivity of materials, the other one comes from the change of interfacial properties for electron conduction, such as micro-cracking and micro-disconnection. To enlighten the mechanism of building high strain gauges, here we analyze the value of GF (or NCC under specifically applied strains) with computer simulation (Equivalent resistor network based on Matlab software). For the PANi and GM/paper sensor, the NCC values were low, which basically remain zero and 2–8 under 2–4% strain respectively. The microscopic images also confirm that there are no structural defects (Figs. S6a–c). In comparison, increasing strain from 5% to 7%, micro-crackings were observed with increased distance between neighboring flakes and decreased overlap areas, leading to higher NCC values (Figs. S6d–f). Therefore, the strain-resistive effects of the PANi and GM/paper sensor are mainly from micro-cracking effect [37,40,45]. With reference to GM/PANi/paper sensor, GM is closely contacted with polyaniline deposited on the filter paper to build the stacked structures.

The formation of GM/PANi composite could favor more electron transport intersections/connections. Applying strain to GM/PANi/paper led to the formation of micro-disconnections and micro-crackings in electron transport intersections/connections under loading 2–4% strain. Under higher strain of 5–7%, the electronic transmission path rapidly disconnected, resulting in a dramatically increase of resistance. Thereby, the value of NCC could reach as higher as to 800 under 7% strain (Fig. 2i). To further validate the assumption of micro-disconnection and micro-cracking effect in GM/PANi/paper sensor, Raman spectroscopy was used to characterize the distribution of GM and PANi in GM/PANi/paper sensor through the analysis of Raman data of large scale (Fig. S7) before and after loading 7% strain. As shown in Fig. 3a–h, many micro-disconnections at GM and PANi interconnections/junctions can be observed after 7% strain loading on GM/PANi/paper (Fig. 3e and f, g and h). Many micro-crackings of GM and PANi were also formed under the 7% strain, the crisscross structure of GM was changed into micro-crisscross structure and lots of micro-crackings after 7% strain loading.

A simulated model of micro-disconnection and micro-cracking was schematized to elucidate the increase of NCCs, as shown in Fig. 4a and Fig. S8. Meanwhile, a schematic model of the current pathway within the GM/PANi sensor was shown in Fig. 4b. In this model, the interfaces between GM and PANi form electrical networks with variable resistors, which further assembled into current pathways. The crossed micro-disconnections and microcrackings could break off the electrical

pathways and lead to the increase of resistance. Considering that the GM with crisscross meshes structure is evenly flatted out on the PANi filter paper, there are many series and parallel circuits of sensor under the testing condition. A Matlab program was developed to simulate the equivalent resistor network and the output of the resistance (Fig. S9). To build this network, GM and PANi were chopped up into many equivalent resistance elements as building blocks. They were connected in parallel or series to form the circuit shown in Fig. 4.

The regulating resistance value of GM and PANi resistance elements is equivalent to the change of GM and PANi's resistance caused by the micro-disconnection and micro-cracking effect. Considering PANi's limited stretchability, the micro-disconnections and micro-crackings in the GM/PANi/paper sensor were randomly distributed under the higher strain (from 5 to 7%). With this model, the resistance of GM/PANi under three strain was calculated. The NCC versus strain for GM/PANi samples of different configurations is illustrated in Fig. 4c, the resistance of the GM/PANi/paper sensor sharply increases with the lots of segments gradually broken one by one or alternately (Fig. S9-1-4). The theoretical value and the experimental value are basically consistent under 2%–4% strain and a little smaller than the experimental value under the strain (5%–7%). Based on the fitting curve of experimental and simulated results, the calculation result of NCCs showed that an exponential increase of NCC when increasing strains, which was in good agreement with the previous experimental results (Fig. S10). Therefore, the formation of microcracks and micro-disconnections in GM/PANi interface could well explain the remarkable resistance change upon the higher strain for GM/PANi/paper sensor.

In addition, compared with other resistive-type strain sensors (Table S2), our strain sensor's NCC or GF could reach 800 or 1.1×10^4 under the 7% strain, which is close to the highest value thus far reported.⁴³ In addition, other resistive-type strain sensors are often composed of thinner layers of graphene with relatively poor mechanical property [46,47], whereas the composite of GM/PANi/paper with thicker graphene layer can greatly improve the transferability from the original substrate to soft device-substrate while keeping the integrity. As for the graphene, the intensity of the G band can be used to determine the number of layers [48,49], the major Raman features of graphene are the so called G band ($\sim 1582.5 \text{ cm}^{-1}$) and 2D band ($\sim 2706 \text{ cm}^{-1}$), the layer of the GM is about ten, as shown in Fig. S11. What's more, the paper-based sensor is more favorable to transfer the graphene meshes due to good hydrophilicity and strong capillary force. To demonstrate the GM/PANi/paper sensor's excellent stability, the sensors were used to evaluate the recovery performance normalized by the conductivity change upon 1000 cycles under 7% strain. The coefficient of variance (CV) for NCC value was expressed in Equation (3):

$$CV = \sigma \div \mu \quad (3)$$

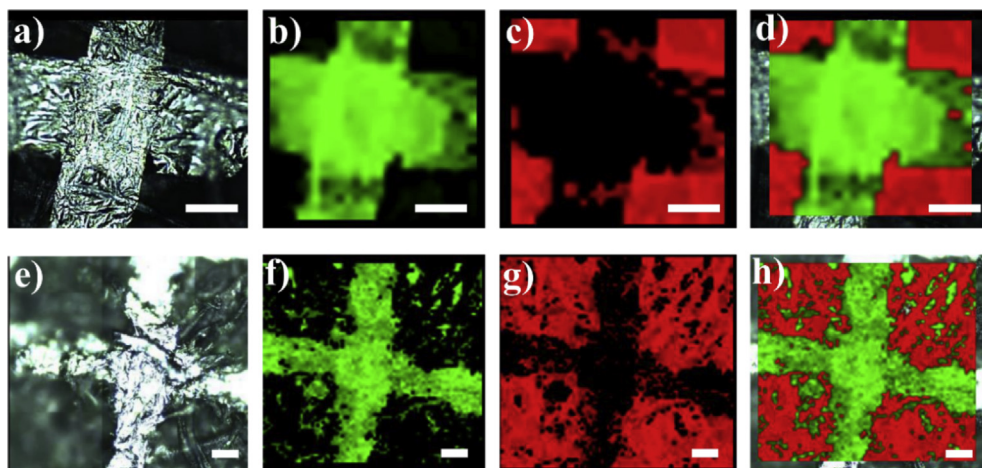


Fig. 3. Raman images of GM/PANi/paper strain sensors, a (under zero applied strain) and e (under 7% strain) were Raman bright field images, b-d and f-h were Raman Mapped images, green cross and red fractures stand for GM and PANi, respectively. Raman Mapped images of GM (b), PANi (c), GM/PANi (d) under zero applied strain and GM (f), PANi (g), GM/PANi (h) under 7% strain were the pictures for component distribution of GM and PANi in the strain sensor, a-d, scale bar: 50 μm , e-h, scale bar: 50 μm . (For interpretation of the references to color in this figure legend, the reader is referred to the Web version of this article.)

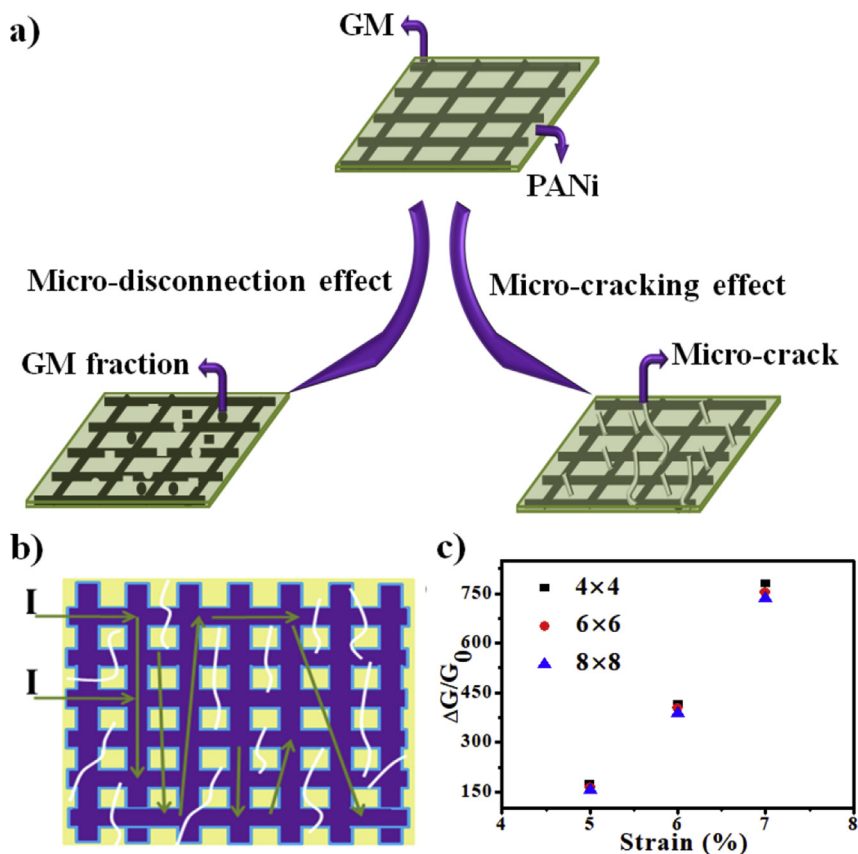


Fig. 4. (a) The strain-resistance response of the sensors from micro-disconnection effect and micro-cracking effect. (b) Current pathway through a fractured sensor. (c) Calculated NCCs of sensors with different configurations.

where σ is the standard deviation of the NCC, μ is the average value of the NCC. The μ of GM/PANi/paper sensor is 747 under 7% strain while σ is 39.1. Although there are slight fluctuations in cycling data, the coefficient of variance (CV) is less than 6% (Fig. S12).

3.4. Wearable strain sensor for sign language “recognition”

Sensing and identifying gestures are two crucial issues to realize gestural user interfaces. Here, taking full advantage of the sensitivity, and flexibility (Fig. S2), PANi/GM paper-based sensors were designed into rectangle-shaped and attached on finger joints for the conductivity measurements. We detected the sensor's NCC induced by different gestures. Three characteristic peaks for finger bending with different ratios are demonstrated in Figs. S13a–c. The NCC value is positively correlated with the bending angle. The strain sensors show fast response when the finger bend and stretch at a frequency of 1 Hz (Fig. S13 d, i). The NCC is up to 750 under 90° bending for the left hand and right hand thumb, corresponding strain were calculated through the length change of the sensors upon bending (Table S3). The NCC of the GM/PANi/paper sensor increased rapidly and drastically under wide bending and stretching. It showed a similar response when the sensor was attached to index finger, middle finger, ring finger or little finger (Fig. S13 e–m). Though the NCC shows a minimum value on middle finger, it still achieved 210 under 90° bending. Therefore, by attaching the sensor on fingers, the characteristic peaks can be applied to the sign language recognition.

Sign language mainly bases on manual communication to convey the thoughts of a speaker by coordinating movement and orientation of hands, arm or body. We utilized the paper-based strain sensor to monitor the finger movement of three kinds of sign language “A”, “B” and “C”, as illustrated in Fig. 5a–d. Recognition of sign language “A” with the strain sensor shows four characteristic peaks corresponding to

the bending of four different fingers other than thumb, giving the results of “01111” (Fig. 5e). Whereas for the recognition of letter “B”, it shows a characteristic peak from thumb movement with four other zero normalized conductivity changes, giving the results of “10000” (Fig. 5f). For the letter “C”, all five fingers bending results in five characteristic peaks, outputting with “11111” as shown in Fig. 5g. With 5 fingers signal combination, we are able to achieve $2^5 = 32$ different outputs which can cover all 26 letters. If we use these sensors to monitor all 10 fingers simultaneously, we will theoretically generate $2^{10} = 1024$ combinations which cover far more than the letters, number and symbols at one time movement. However, for some commonly used words such as “Thanks”, one may simplify the finger movements. For instance, thumb moving twice can be interpreted as “Thanks”. In addition, the combination of wrist bending may be included for sign language recognition as well, such as “goodbye”, expressed as waving of the hand which relies on the wrist twist without any bending of fingers (Fig. S14).

Real time detection and data transmission are important features for remote and personalized human monitoring and should be integrated into one single platform. In order to validate the potential of our sensor for the interpretation of communication between healthy individuals and deaf-mute person, we made a preliminary attempt, in which the physiological and environment data were first gathered from human body by the wearable sensors, then wireless or internet communications were further employed to transmit the collected data to a mobile phone, which were present in Fig. S15 and Movie 1. However, the raw data is five data streams from five fingers, and it inevitably varies among different users. To improve the robustness of the system and make it user-friendly, a neural-network-based interpretation module was developed to translate the sensor data of different gestures into natural language. The structure of the neural network is illustrated in Fig. S15. As proof of the concept, the recognition of gesture “thank you” can be accurately

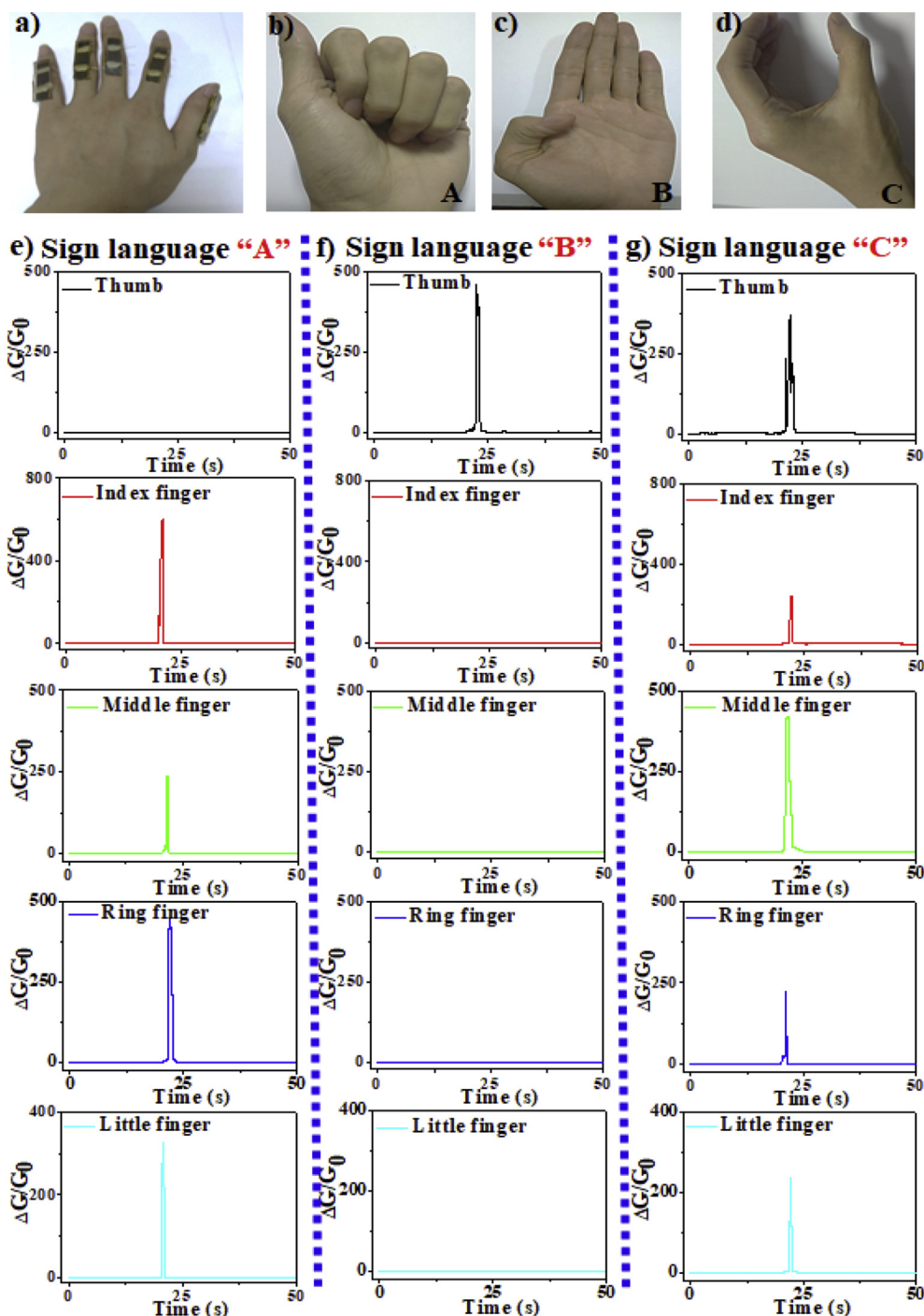


Fig. 5. Wearable strain sensor for sign language “recognition”. Photograph of the thumb finger with sensors (a). Photographs of the five fingers bending for sign language letter “A” (b), letter “B” (c), sign language “C” (d). The NCC of strain sensors for sign language “A” (e), sign language “B” (f), sign language “C” (g).

realized in the neural network module.

Supplementary video related to this article can be found at <https://doi.org/10.1016/j.compscitech.2019.05.017>.

4. Conclusions

We demonstrated a straightforward and generally applicable pen-writing, paper-transferring and elastomer-packaging approach for the fabrication of a strain sensor. This innovative strain sensor with sandwich structure is cost-effective with ultra-high strain sensitivity, large flexibility and good stability. The ultra-sensitivity of the sensors is mainly ascribed to micro-disconnection effect and micro-cracking effect

of GM and PANi. This wearable and flexible strain sensors showed feasibility for sign language recognition based on the monitoring of finger movements. Future work will include the development of multi-channel strain sensors to monitor multiple movements of joints other than fingers for more complicated sign language or other health applications. We believe that this technology can be employed as an excellent candidate to help people with speech and hearing impairment.

Acknowledgments

This research is financially supported by the Natural Science Foundation of China (NSFC-21573162, 21603166, 201605116,

21773172), WIBEZD2014001-02 and Wenzhou Public Welfare Science and Technology Project (S20170015).

Appendix A. Supplementary data

Supplementary data to this article can be found online at <https://doi.org/10.1016/j.compscitech.2019.05.017>.

References

- [1] S. Yao, P. Swetha, Y. Zhu, Nanomaterial-enabled wearable sensors for healthcare, *Adv. Healthc. Mater.* 7 (2018) 1700889.
- [2] Y. Lee, J. Kim, H. Joo, M.S. Raj, R. Ghaffari, D.H. Kim, Wearable sensing systems with mechanically soft assemblies of nanoscale materials, *Adv. Mater. Technol.* 2 (2017) 1700053.
- [3] T.X. Gong, H. Zhang, W. Huang, L.N. Mao, Y.Z. Ke, M. Gao, B. Yu, Highly responsive flexible strain sensor using polystyrene nanoparticle doped reduced graphene oxide for human health monitoring, *Carbon* 140 (2018) 286–295.
- [4] Y. Liu, M. Pharr, G.A. Salvatore, Lab-on-skin: a review of flexible and stretchable electronics for wearable health monitoring, *ACS Nano* 11 (2017) 9614–9635.
- [5] J.M. Nassar, K. Mishra, K. Lau, A. Aguirre-Pablo, M.M. Hussain, Recyclable non-functionalized paper-based ultralow-cost wearable health monitoring system, *Adv. Mater. Technol.* 2 (2017) 1600228.
- [6] Z. Bao, X. Chen, Flexible and stretchable devices, *Adv. Mater.* 28 (2016) 4177–4179.
- [7] D. Kang, P.V. Pikhitsa, Y.W. Choi, C. Lee, S.S. Shin, L. Piao, B. Park, K.Y. Suh, T. Kim, M. Choi, Ultrasensitive mechanical crack-based sensor inspired by the spider sensory system, *Nature* 516 (2014) 222–226.
- [8] F. Güder, A. Ainla, J. Redston, B. Mosadegh, A. Glavan, T.J. Martin, G.M. Whitesides, Paper-based electrical respiration sensor, *Angew. Chem. Int. Ed.* 55 (2016) 5727–5732.
- [9] F. Zhang, Y. Zang, D. Huang, C. Di, D. Zhu, Flexible suspended gate organic thin-film transistors for ultra-sensitive pressure detection, *Nat. Commun.* 6 (2015) 6269.
- [10] D. Jevtics, A. Hurtado, B. Guilhabert, J. McPhillimy, G. Cantarella, Q. Gao, H.H. Tan, C. Jagadish, M.J. Strain, M.D. Dawson, Integration of semiconductor nanowire lasers with polymeric waveguide devices on a mechanically flexible substrate, *Nano Lett.* 17 (2017) 5990–5994.
- [11] C. Liao, M. Zhang, M.Y. Yao, T. Hua, L. Li, F. Yan, Flexible organic electronics in biology: materials and devices, *Adv. Mater.* 27 (2015) 7493–7527.
- [12] S.H. Jeong, S. Zhang, K. Hjort, J. Hilborn, Z. Wu, Stretchable electronic devices: PDMS-based elastomer tuned soft, stretchable, and sticky for epidermal electronics, *Adv. Mater.* 28 (2016) 5830–5836.
- [13] A. Gerratt, H. Michaud, S.P. Lacour, Elastomeric electronic skin for prosthetic tactile sensation, *Adv. Funct. Mater.* 25 (2015) 2287–2295.
- [14] Y. Jiang, Z. Liu, N. Matsuhisa, D. Qi, W.R. Leow, H. Yang, J. Yu, G. Chen, Y. Liu, C. Wan, Z. Liu, X.D. Chen, Auxetic mechanical metamaterials to enhance sensitivity of stretchable strain sensors, *Adv. Mater.* 30 (2018) 1706589.
- [15] M.D. Ho, Y. Ling, L.W. Yap, Y. Wang, D. Dong, Y. Zhao, W. Cheng, Percolating network of ultrathin gold nanowires and silver nanowires toward invisible wearable sensors for detecting emotional expression and apexcardiogram, *Adv. Funct. Mater.* 27 (2017) 1700845.
- [16] C. Yan, J. Wang, W. Kang, M. Cui, X. Wang, C.Y. Foo, K.J. Chee, P.S. Lee, Highly stretchable piezoresistive graphene–nanocellulose nanopaper for strain sensors, *Adv. Mater.* 26 (2014) 2022–2027.
- [17] J.T. Muth, D.M. Vogt, R.L. Truby, Y. Mengüç, D.B. Kolesky, R.J. Wood, J.A. Lewis, Embedded 3D printing of strain sensors within highly stretchable elastomers, *Adv. Mater.* 26 (2014) 6307–6312.
- [18] C.S. Boland, U. Khan, C. Backes, A. O'Neill, J. McCauley, S. Duane, R. Shanker, Y. Liu, I. Jurewicz, A.B. Dalton, J.N. Coleman, Sensitive, high-strain, high-rate bodily motion sensors based on graphene–rubber composites, *ACS Nano* 8 (2014) 8819–8830.
- [19] H. Yang, X.F. Yao, Z. Zhang, L. Gong, L. Yuan, Y. Yuan, Y.H. Liu, Highly sensitive and stretchable graphene–silicone rubber composites for strain sensing, *Compos. Sci. Technol.* 167 (2018) 371–378.
- [20] G. Cai, J. Wang, K. Qian, J. Chen, S. Li, P.S. Lee, Extremely stretchable strain sensors based on conductive self-healing dynamic cross-links hydrogels for human-motion detection, *Adv. Sci.* 4 (2017) 1600190.
- [21] B. Zhang, J. Lei, D. Qi, Z. Liu, Y. Wang, G. Xiao, J. Wu, W. Zhang, F. Huo, X. Chen, Stretchable conductive fibers based on a cracking control strategy for wearable electronics, *Adv. Funct. Mater.* 28 (2018) 1801683.
- [22] Y. Ma, M. Pharr, L. Wang, J. Kim, Y. Liu, Y. Xue, R. Ning, X. Wang, H.U. Chung, X. Feng, J.A. Rogers, Y. Huang, Soft elastomers with ionic liquid-filled cavities as strain isolating substrates for wearable electronics, *Small* 13 (2017) 1602954.
- [23] T.Q. Trung, N.E. Lee, Flexible and stretchable physical sensor integrated platforms for wearable human-activity monitoring and personal healthcare, *Adv. Mater.* 28 (2016) 4338–4372.
- [24] Y. Wang, J. Hao, Z. Huang, G.Q. Zheng, K. Dai, C. Liu, C. Shen, Flexible electrically resistive-type strain sensors based on reduced graphene oxide-decorated electrospun polymer fibrous mats for human motion monitoring, *Carbon* 126 (2018) 360–371.
- [25] S.L. Zhang, Y.C. Lai, X. He, R. Liu, Y. Zi, Z.L. Wang, Auxetic foam-based contact-mode triboelectric nanogenerator with highly sensitive self-powered strain sensing capabilities to monitor human body movement, *Adv. Funct. Mater.* 27 (2017) 1606695.
- [26] R. Moriche, A. Jiménez-Suárez, M. Sánchez, S.G. Prolongo, A. Ureña, Graphene nanoplatelets coated glass fibre fabrics as strain sensors, *Compos. Sci. Technol.* 126 (2017) 59–64.
- [27] J. Cao, C. Lu, J. Zhuang, M. Liu, X. Zhang, Y. Yu, Q. Tao, Multiple hydrogen bonding enables the self-healing of sensors for human–machine interactions, *Angew. Chem. Int. Ed.* 129 (2017) 8921–8926.
- [28] M. Zhang, C. Wang, H. Wang, M. Jian, X. Hao, Y. Zhang, Carbonized cotton fabric for high-performance wearable strain sensors, *Adv. Funct. Mater.* 27 (2017) 1604795.
- [29] J. Zhao, S. Han, Y. Yang, R. Fu, Y. Ming, C. Lu, H. Liu, H. Gu, Passive and space-discriminative ionic sensors based on durable nanocomposite electrodes toward sign language recognition, *ACS Nano* 11 (2017) 8590–8599.
- [30] C. Wang, X. Li, E. Gao, M. Jian, K. Xia, Q. Wang, Z. Xu, T. Ren, Y. Zhang, Carbonized silk fabric for ultra-stretchable, highly sensitive, and wearable strain sensors, *Adv. Mater.* 28 (2016) 6640–6648.
- [31] S. Lim, D. Son, J. Kim, Y.B. Lee, J.K. Song, S. Choi, D.J. Lee, J.H. Kim, M. Lee, T. Hyeon, D.H. Kim, Transparent and stretchable interactive human machine interface based on patterned graphene heterostructures, *Adv. Funct. Mater.* 25 (2015) 375–383.
- [32] L. Cai, S. Zhang, Y. Zhang, J. Li, J. Miao, Q. Wang, Z. Yu, C. Wang, Direct printing for additive patterning of silver nanowires for stretchable sensor and display applications, *Adv. Mater. Technol.* 3 (2018) 1700232.
- [33] B.U. Hwang, J.H. Lee, T.Q. Trung, E. Roh, D. Il Kim, S.W. Kim, N.E. Lee, Transparent stretchable self-powered patchable sensor platform with ultrasensitive recognition of human activities, *ACS Nano* 9 (2015) 8801–8810.
- [34] X. Gu, L. Shaw, K. Gu, M.F. Toney, Z. Bao, The meniscus-guided deposition of semiconducting polymers, *Nat. Commun.* 9 (2018) 534.
- [35] G. Wang, A. Gasperini, Z. Bao, Stretchable polymer semiconductors for plastic electronics, *Adv. Electron. Mater.* 4 (2018) 1700429.
- [36] Y. Deng, J. Sun, H. Jin, M. Khatib, X. Li, Z. Wei, F. Wang, Y.D. Horev, W. Wu, H. Haick, Volatile organic compounds: chemically modified polyaniline for the detection of volatile biomarkers of minimal sensitivity to humidity and bending, *Adv. Healthc. Mater.* 7 (2018) 1870059.
- [37] J. Cai, C. Zhang, A. Khan, C. Liang, W.D. Li, Highly transparent and flexible polyaniline mesh sensor for chemi-resistive sensing of ammonia gas, *RSC Adv.* 8 (2018) 5312–5320.
- [38] X. Gong, G.T. Fei, W.B. Fu, M. Fang, X.D. Gao, B.N. Zhong, L. Zhang, Flexible strain sensor with high performance based on PANI/PDMS Films, *Org. Electron.* 47 (2017) 51–56.
- [39] E. Roh, B.U. Hwang, D. Kim, B.Y. Kim, N.E. Lee, Stretchable, transparent, ultra-sensitive, and patchable strain sensor for human–machine interfaces comprising a nanohybrid of carbon nanotubes and conductive elastomers, *ACS Nano* 9 (2015) 6252–6261.
- [40] S. Gong, D.T.H. Lai, Y. Wang, L.W. Yap, K.J. Si, Q. Shi, N.N. Jason, T. Sridhar, H. Uddin, W. Cheng, Tattoo-like polyaniline microparticle-doped gold nanowire patches as highly durable wearable sensors, *ACS Appl. Mater. Interfaces* 7 (2015) 19700–19708.
- [41] X. Yu, H. Cheng, M. Zhang, Y. Zhao, L. Qu, G. Shi, Graphene-based smart materials, *Nat. Rev. Mater.* 2 (2017) 17046.
- [42] B. Zhu, Z.Q. Niu, H. Wang, W.R. Leow, H. Wang, Y.G. Li, L.Y. Zheng, J. Wei, F.W. Huo, X.D. Chen, Microstructured graphene arrays for highly sensitive flexible tactile sensors, *Small* 10 (2014) 3625–3631.
- [43] K. Xia, C. Wang, M. Jian, Q. Wang, Y.Y. Zhang, CVD growth of fingerprint-like patterned 3D graphene film for an ultrasensitive pressure sensor, *Nano Res* 11 (2018) 1124–1134.
- [44] J.H. Je, J.M. Kim, J. Jaworski, Progression in the fountain pen approach: from 2D writing to 3D free-form micro/nanofabrication, *Small* 13 (2017) 1600137.
- [45] M. Zhu, Y. Huang, H. Li, Z. Wang, Z. Pei, Q. Xue, H. Geng, C. Zhi, Highly durable, transferable, and substrate-versatile high-performance all-polymer micro supercapacitor with plug-and-play function, *Adv. Mater.* 29 (2017) 1605137.
- [46] J. Kang, D. Shin, S. Bae, B.H. Hong, Graphene transfer: key for applications, *Nanoscale* 4 (2012) 5527–5537.
- [47] J. Rafiee, X. Mi, H. Gullapalli, A.V. Thomas, F. Yavari, Y. Shi, P.M. Ajayan, N.A. Koratkar, Wetting transparency of graphene, *Nat. Mater.* 11 (2012) 217–222.
- [48] H. Koratkar, Y. Wang, X. Cao, M. Feng, G. Lan, Vibrational properties of graphene and graphene layers, *J. Raman Spectrosc.* 40 (2009) 1791–1796.
- [49] A.C. Ferrari, D.M. Basko, Raman spectroscopy as a versatile tool for studying the properties of graphene, *Nat. Nanotechnol.* 8 (2013) 235–246.